RAA 2018 Vol. **18** No. **3**, 32(14pp) doi: 10.1088/1674–4527/18/3/32

http://www.raa-journal.org *http://iopscience.iop.org/raa*

***R**esearch in*
***A**stronomy and*
***A**strophysics*

New open cluster candidates discovered in the XSTPS-GAC survey

Jin-Cheng Guo[1,2,3,⋆], Hua-Wei Zhang[1,2], Hui-Hua Zhang[1,2], Xiao-Wei Liu[4,1,2], Hai-Bo Yuan[5], Yang Huang[4,1,2,⋆], Song Wang[3], Li Chen[6], Hai-Bin Zhao[7], Ji-Feng Liu[3], Bing-Qiu Chen[4], Mao-Sheng Xiang[3,⋆], Zhi-Jia Tian[1,2,⋆], Zhi-Ying Huo[3] and Chun Wang[1,2]

[1] Department of Astronomy, Peking University, Beijing 100871, China; *jincheng.guo@pku.edu.cn;zhanghw@pku.edu.cn*
[2] Kavli Institute for Astronomy and Astrophysics, Peking University, Beijing 100871, China
[3] Key Laboratory of Optical Astronomy, National Astronomical Observatories, Chinese Academy of Sciences, Beijing 100012, China
[4] South-Western Institute for Astronomy Research, Yunnan University, Kunming 650500, China
[5] Department of Astronomy, Beijing Normal University, Beijing 100875, China
[6] Shanghai Astronomical Observatory, Chinese Academy of Sciences, Shanghai 200030, China
[7] Purple Mountain Observatory, Chinese Academy of Sciences, Nanjing 210008, China

Received 2017 November 10; accepted 2017 December 28

Abstract The Xuyi Schmidt Telescope Photometric Survey of the Galactic Anti-center (XSTPS-GAC) is a photometric sky survey that covers nearly 6000 deg^2 towards the Galactic Anti-center (GAC) in the g, r, i bands. Half of its survey field is located on the Galactic Anti-center disk, which makes XSTPS-GAC highly suitable to search for new open clusters in the GAC region. In this paper, we report new open cluster candidates discovered in this survey, as well as properties of these open cluster candidates, such as age, distance and reddening, derived by isochrone fitting in the color-magnitude diagram (CMD). These open cluster candidates are stellar density peaks detected in the star density maps by applying the method from Koposov et al. Each candidate is inspected in terms of its true color image composed from three XSTPS-GAC band images. Then its CMD is checked, in order to identify whether the central region stars have a clear isochrone-like trend differing from background stars. The parameters derived from isochrone fitting for these candidates are mainly based on three band photometry of XSTPS-GAC. Moreover, when these new candidates are able to be seen clearly in 2MASS data, their parameters are also derived based on the 2MASS $(J - H, J)$ CMD. There are a total of 320 known open clusters rediscovered and 24 new open cluster candidates discovered in this work. Furthermore, the parameters of these new candidates, as well as another 11 previously known open clusters, are properly determined for the first time.

Key words: open clusters and associations: general — Galaxy: structure — methods: data analysis

1 INTRODUCTION

It is commonly accepted that star clusters are the building blocks of a galaxy. They are the environment where most star birth occurs (Lada & Lada 2003; de Wit et al. 2005). Thus, star clusters play an important role in investigations of star formation and stellar evolution, and can be used as tracers of structure and evolution in their host galaxy. Since star clusters usually contain tens to thousands of stars with single-age and single-metallicity, their determined fundamental parameters, such as age, distance and reddening, can be more accurate and reliable. Moreover, a star cluster is a natural laboratory to test the validation of spectroscopic methods that are used

⋆ LAMOST Fellow

to determine stellar parameters like $T_{\rm eff}$, $\log\ g$ and metallicity, as in Xiang et al. (2015).

There are 2167 open clusters in the most recent version (2016 Jan 28) of the DAML02 catalog (Dias et al. 2002). These clusters are collected from various literature, therefore, they are based on different observations and their cluster parameters are derived by different methods. Kharchenko et al. (2012, 2013) collect 3784 clusters from the literature in their Milky Way Star Clusters (MWSC) catalog, including open clusters, globular clusters, embedded clusters and star associations. Homogeneous cluster parameters have been determined for 3006 clusters, using 2MASS (Skrutskie et al. 2006) photometry combined with position and proper motions from PPMXL (Roeser et al. 2010). However, the number of known star clusters in the Milky Way is still much less than the number predicted by related theories, which is more than 20 000 (Portegies Zwart et al. 2010; Bonatto & Bica 2006).

Many large area sky surveys have been used to find clusters and derive cluster parameters. Among those surveys, 2MASS, SDSS and DSS are the most useful ones, adopted by the work of Bonatto & Bica (2006), Bica et al. (2006), An et al. (2009) and Kronberger et al. (2006). Recently, Borissova et al. (2011) used data from VISTA Variables in the Via Lactea (VVV) survey (Minniti et al. 2010) to find new open clusters in the Galactic center region, which suffers serious dust extinction. VVV was also used to improve the accuracy of cluster parameters (Majaess et al. 2012). On the other hand, large astrometric catalogs, such as UCAC4 (Zacharias et al. 2013), GSC2.3 (Lasker et al. 2008) and PPMXL (Roeser et al. 2010), compiled from various sky surveys could provide position and proper motion with high precision. Proper motion is the most important information to identify member stars in a cluster (Kharchenko et al. 2005).

In the early days, bright open clusters were discovered by eye. For some large and loose clusters, they were found by proper motion analysis. Nowadays, new effective methods have been developed to find more clusters. For example, more and more clusters have been discovered by automatic methods. Froebrich et al. (2007) found 1021 clusters based on stellar density maps from the 2MASS point source catalog, which greatly increased the sample of known clusters. Koposov et al. (2008) constructed a 2D filter based on the difference between two Gaussian profiles. By convolving the stellar density map with this filter, cluster candidates were found more effectively.

The Xuyi Schmidt Telescope Photometric Survey of the Galactic Anti-center (XSTPS-GAC) is a large sky survey in SDSS g, r, i bands. It is the photometric part of the Digital Sky Survey of the Galactic Anti-center (DSS-GAC, Liu et al. 2015), and DSS-GAC is a photometric and spectroscopic sky survey (Liu et al. 2014). A significant part of the LAMOST survey (Zhao et al. 2012) is the spectroscopic part of DSS-GAC. XSTPS-GAC covers a continuous sky area of over 6000 $\deg^2$ towards the Galactic Anti-center (GAC). Nearly half of XSTPS-GAC's survey field is located on the GAC disk, which makes XSTPS-GAC highly suitable to search for new open clusters in the GAC region. Compared to 2MASS, which currently is the main catalog used to find open clusters, XSTPS-GAC reaches a deeper limiting magnitude of $r \approx 19.0$ mag. This fact will lead to more observations of distant faint stars, which would also suffer heavier dust extinction. Therefore, we expect to discover new open clusters from XSTPS-GAC photometric data.

The paper is organized as follows. In Section 2, we briefly present the observations and data reduction of XSTPS-GAC. The method to search for cluster candidates is described in Section 3. We present results and discussion on interesting clusters in Section 4. Finally, we give the conclusions in Section 5.

2 OBSERVATION AND DATA REDUCTION

The XSTPS-GAC started collecting data in October 2009 and completed in March 2011, using the Xuyi Schmidt telescope operated by Purple Mountain Observatory, Chinese Academy of Sciences. The telescope has a 120 cm primary mirror and a 104 cm correction plate. A 4096×4096 CCD camera is mounted on the telescope, with a $1.94^{\rm o}\times1.94^{\rm o}$ effective field-of-view and a pixel scale of 1.705 arcsec. Seeing at the site can reach up to $1''$ under the best air conditions. During the XSTPS-GAC operation period, the mean atmospheric extinction coefficients are 0.69, 0.55 and 0.38 mag/airmass for the g, r, i bands, respectively. The typical night sky brightness could attain 21.7, 20.8 and 20.0 mag arcsec^{-2} for these three bands (Zhang et al. 2013).

XSTPS-GAC collected more than 20 000 CCD images in the g, r, i bands, covering a continuous GAC area from 3 h to 9 h in right ascension, and from -10° to +60° in declination, plus an extended area of about 900 deg^2 towards M31/M33. We designed 39 observation stripes

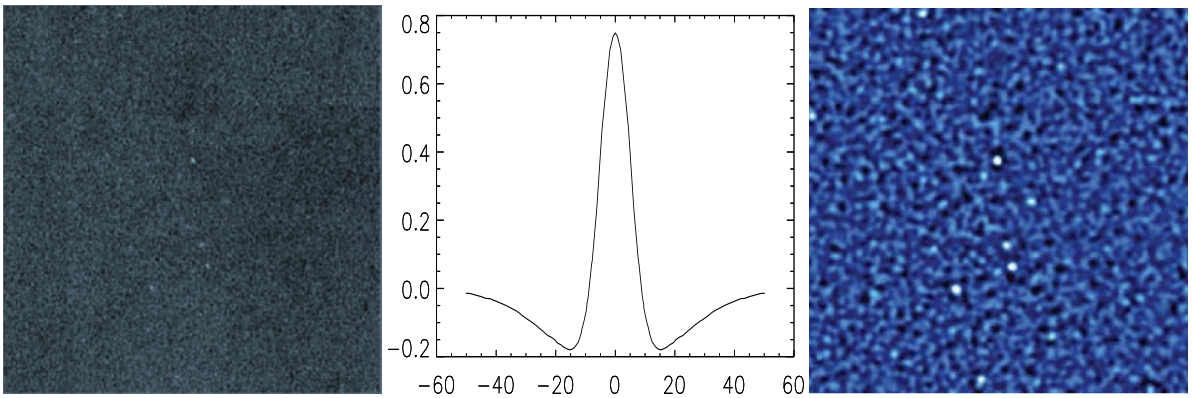

Fig. 1 The *Koposov* method was adopted to search for an overdensity area. The *left panel* is the stellar number density map based on data from XSTPS-GAC. The constructed *Koposov* filter is displayed in the *middle panel*. The *right panel* shows the stellar number density map after convolution. The overdensity area is more evident.

to cover the whole GAC region. Each stripe consists of a group of continuous fields under a fixed declination, and each field has a 0.95 deg^2 area, about half of a field, overlapping with its adjacent fields in the same stripe. As a result, a single source in the XSTPS-GAC planned region has been exposed at least two times for each band. The observations were carried out by adopting 90 s as exposure time, using only one filter for each night and observing two stripes together. This observing strategy not only enabled the observation to match the sky moving speed well, but also ensured consistency over a whole night of observations in the sense of airmass.

Data reduction was carefully carried out, including overscan trimming, bias correction, flat-fielding, source detection and subtraction in typical DAOPHOT (Stetson 1987) steps for CCD images. Flat-fielding is accomplished by applying the super-sky-flat (SSF) method, which assumes the sky background is homogeneous. The SSF field of each night was subtracted from hundreds of raw observed fields in the same filter. Comparing with a dome flat or twilight flat, which may suffer from streaks, non-linearity and large-scale inhomogeneities on the field, our SSF field correction accuracy could reach 1%. We also divided one CCD image into 5×5 subfields, in order to construct the star point-spread-function (PSF) more precisely, which ensures robust PSF flux measurement for all detected stars. Based on the large overlapping area between adjacent fields, the photometry calibration was done in the UberCal calibration manner, in the same way as for SDSS (Padmanabhan et al. 2008). The typical photometric accuracy could reach up to 0.03 mag (Yuan et al. 2017, in preparation). By adopting PPMXL as the astrometric reference, the astrometric accuracy could reach 70 mas for stars brighter than 17.0 mag, and better than 200 mas for stars at the faint end (~ 19.0 mag) of the survey (Zhang et al. 2014).

3 CLUSTER SEARCH AND ANALYSIS

3.1 Candidate Search

We applied the method from Koposov et al. (2008) to detect high stellar density regions in XSTPS-GAC. First, a stellar density map was constructed based on each CCD image, which could improve the speed of convolution in the following process. Stars are counted in a grid size of 10×10 CCD pixels, namely $17.5 \times 17.5\,\mathrm{arcsec}^2$. The selection of this grid size is a result of considering two situations. One, if a larger grid size is chosen, small scale density variation would be neglected. On the other hand, if a smaller grid size is chosen, there would be many zero counts. In addition, we selected stars that at least have r and i band measurements, since the g band suffers from relatively heavier dust extinction, and more stars are able to be detected in the r and i bands. Also we constrained the photometric error to be less than 0.1 mag, ensuring the photometric quality. The filter from Koposov et al. (2008) was adopted in this work, shown in Equation (1).

$$S(ra, dec) = \sqrt{4\pi}\sigma_1 \frac{M(ra, dec) * (G(ra, dec, \sigma_1) - G(ra, dec, \sigma_2))}{\sqrt{M(ra, dec) * G(ra, dec, \sigma_2)}}, \quad (1)$$

where $M(ra, dec)$ represents the star number density map, while $G(ra, dec, \sigma)$ is the circular 2D Gaussian with unity integral and width of σ.

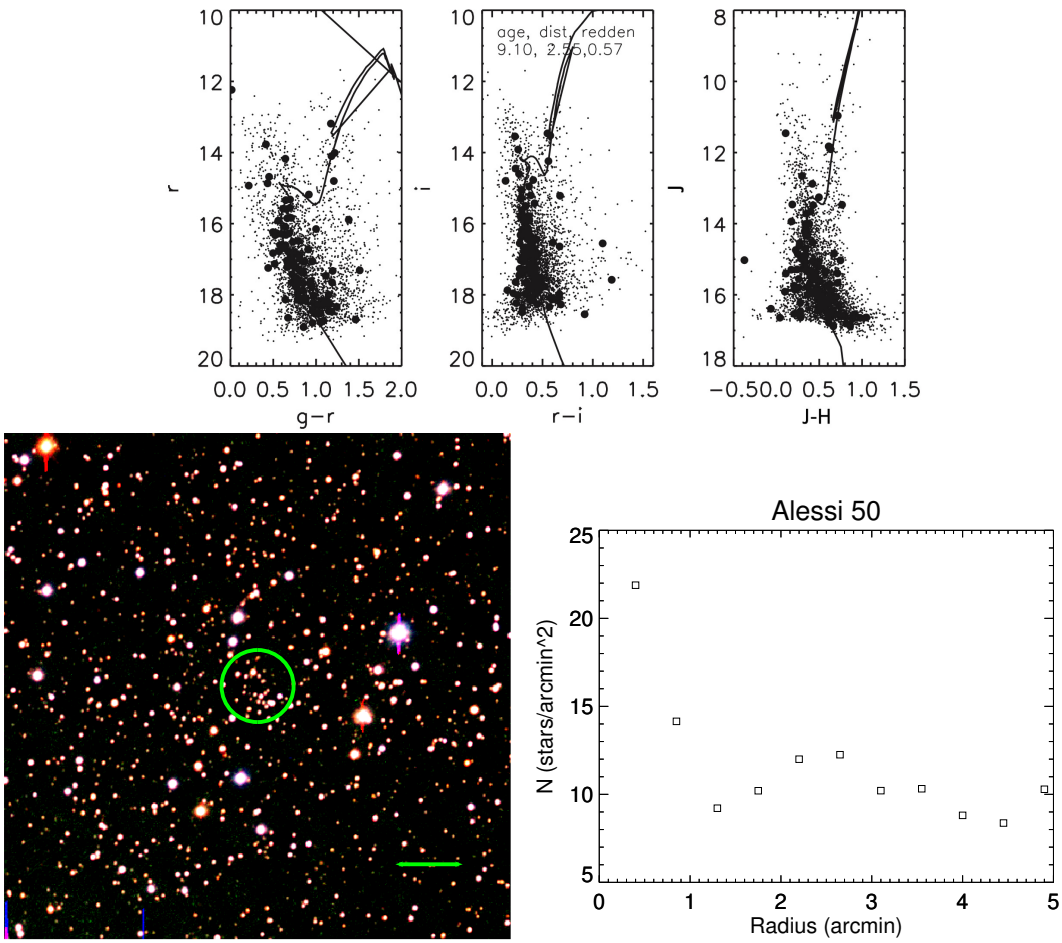

Fig. 2 CMDs, true color image and RDP for cluster Alessi 50. The *top three panels* are CMDs, while *bottom left* is a true color CCD image, and RDP is at the *bottom right*. The three CMDs are the $(r, g-r)$, $(i, r-i)$ and 2MASS $(J, J-H)$ diagrams. The *black filled circles* on each CMD are the stars within cluster visual radius which are calculated by radial profile fitting, as described in Sect. 3.2, and the *background dots* are the comparison field stars. Each true color image was combined by the g, r, i band $15' \times 15'$ XSTPS-GAC image centered on the cluster center, and the cluster core radius $R_{\rm core}$ is marked by a circle. The line at the lower right is a $2'$ scale. Here and for each cluster in subsequent figures, the determined log(*age*) is labeled on its $(i, r-i)$ CMD.

The convolved map $S(ra, dec)$ shows the deviation of $M(ra, dec) * G(ra, dec, \sigma_1)$ above the background estimation, namely $M(ra, dec) * G(ra, dec, \sigma_2)$. The overdensity detections on this map can be easily acquired by setting $S(ra, dec) > 5$, which represents overdensity statistical significance above 5σ. The 1D slice of the 2D filter with convolution for $\sigma_1 = 3'$ and $\sigma_2 = 6'$ is shown in Figure 1, similar to the filter from Koposov et al. (2008). In this work, $S(ra, dec) > 4.5$, $\sigma_1 = 2'$ and $\sigma_2 = 6'$ were used, in order to include more small-sized clusters.

Due to the fact that half of each XSTPS-GAC plate overlaps with adjacent ones, the true density peaks will be detected at least two times. In this sense, density peaks produced by the edge effect can be easily removed. However, after removing the edge effect, we still found lots of density peaks in relatively high Galactic latitude regions. Some of them could be real star clusters, but a significant number of these detections should be caused by field star number density fluctuations. According to Gilmore & Reid (1983), star density decreases along with Galactic latitude in a power-law manner. Therefore, in the low latitude dense region populated by field stars, the density variation feature of true star clusters will be less significant. While in the relatively high latitude sparse region, many overdensity detections are in fact due to the magnification of star density fluctuation. In order to find more true cluster overdensity detections in the Galactic plane with relatively low significance and reduce false detections caused by star density fluctuations in the higher latitude region, corrections are carefully

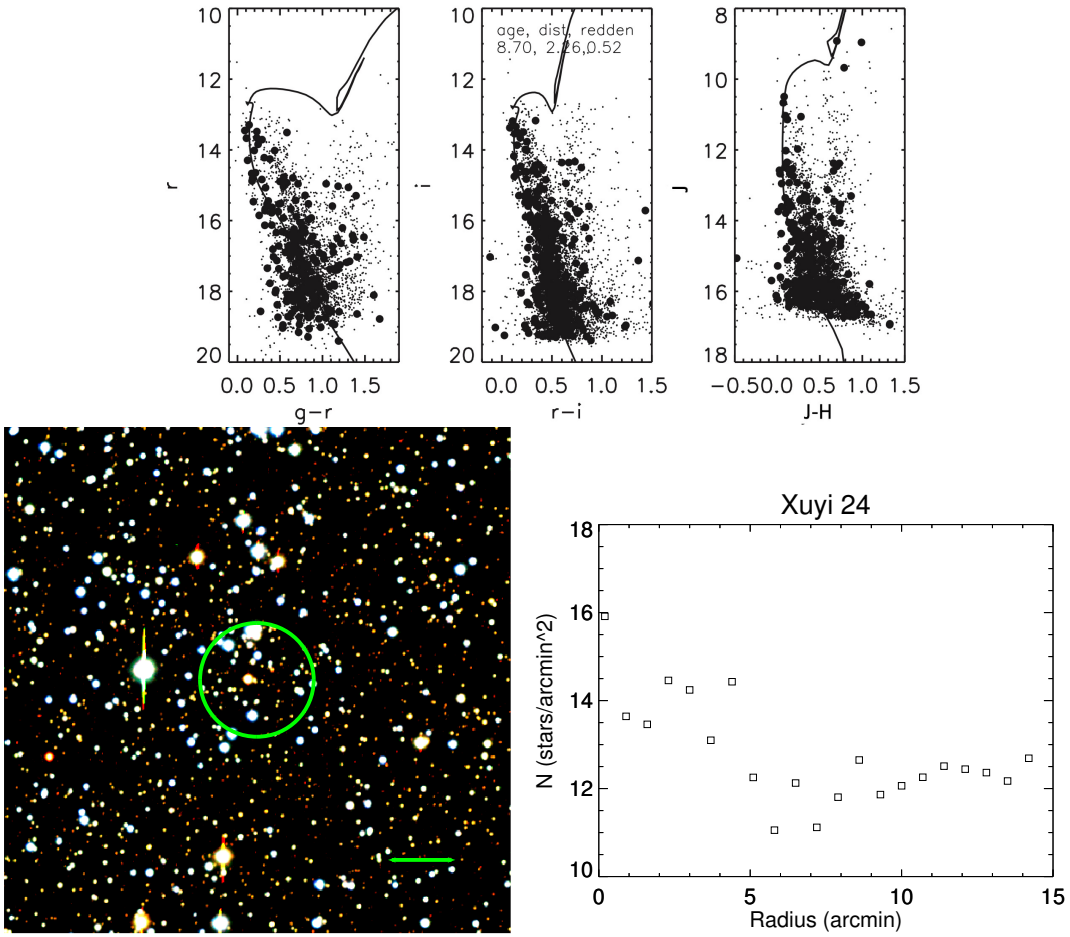

Fig. 3 Same as Fig. 2 but for cluster Xuyi 24. It is also an example of the second kind of obvious cluster that is relatively compact.

made as described in the following procedures. First, we adopted the square root of the star density in each density peak as the weight for this peak, which could help to strengthen the significance of low latitude peaks. Second, the majority of known clusters, from either MWSC or DAML02, are located in the interval of Galactic latitude $-20^\circ < b < 20^\circ$. Thus, regions outside this interval are not considered in our work. Third, peaks with low star counts are excluded as well. Finally, there are 1 921 density peaks detected above the weighted detection threshold, which is 4.5 σ.

After these overdensity peaks were selected, each peak was examined with its $1^\circ \times 1^\circ$ true color image built from XSTPS-GAC three-band CCD images. For a real cluster, member stars will spatially concentrate in the true color image. Furthermore, the distribution of cluster member stars on the color-magnitude diagram (CMD) should follow an isochrone-like trend. Finally, there are 320 known open clusters, either in DAML02 or MWSC, that were rediscovered. However, 12 of these known clusters, mainly discovered by Kronberger et al. (2006), were only cataloged by their celestial coordinates without any physical parameters. Among other detected unknown peaks, there are 30 peaks classified as high probability new cluster candidates.

In the following analysis, our newly discovered cluster candidates and 12 other known clusters are studied together. The new clusters will be named by the word $Xuyi$ with a suffix number that represents their discovery order. While for known clusters, the original names are still used here. All clusters have an IAU-recognized format DSH Jhhmm.m±ddmm ID assigned.

3.2 Fundamental Parameters

In this work, the most concentrated place of star cluster members, i.e. the highest number density point, is considered as the cluster center. We iteratively calculated the mode of star coordinates in a selected 30×30 arcmin^2

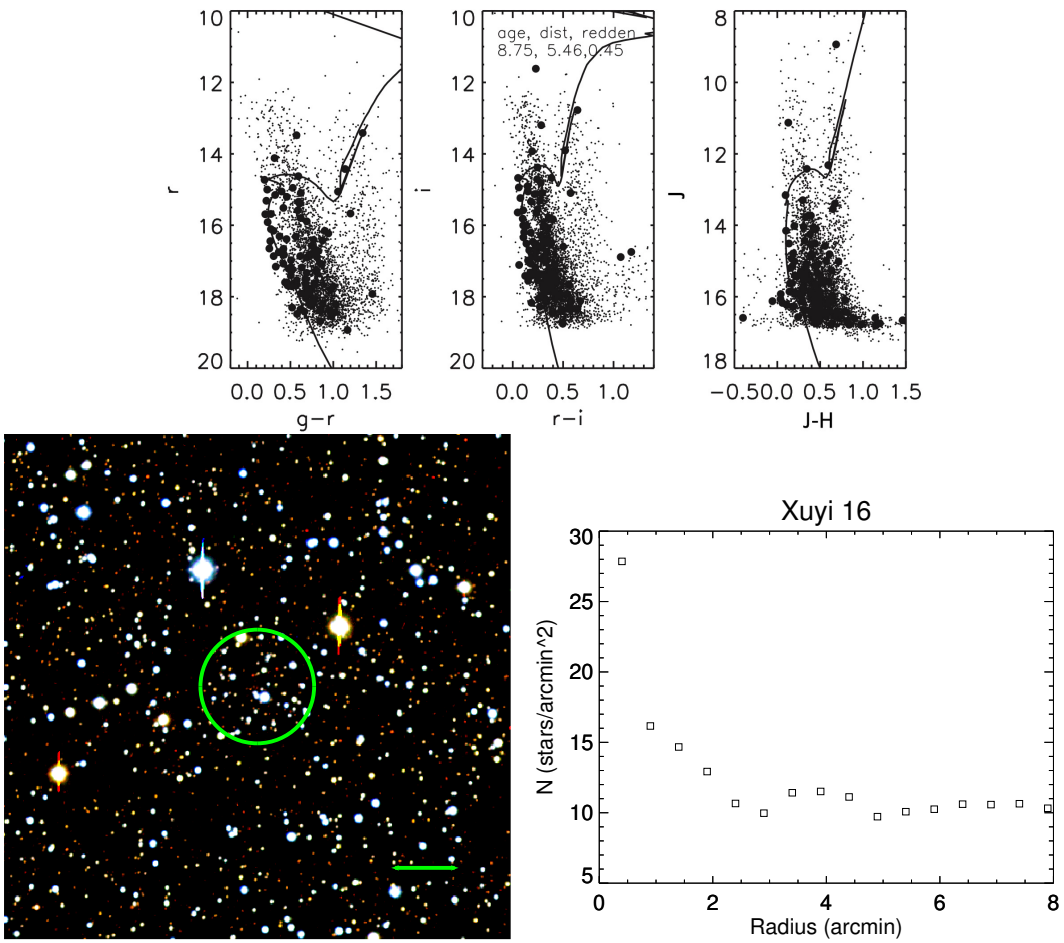

Fig. 4 Same as Fig. 2 but for cluster Xuyi 16. It is an example of an obvious cluster that shows a clear blue main sequence.

region. The mode defined in the SE$_{\rm XTRACTOR}$ software (Bertin & Arnouts 1996) is adopted here, as shown in Equation (2).

$$\mathrm{Mode} = 2.5 \times \mathrm{Median} - 1.5 \times \mathrm{Mean}, \qquad (2)$$

where Median is the median value of star coordinates in the selected field, and Mean is the mean value of star coordinates.

After accurate estimations of the cluster central coordinates were obtained, we created a radial density profile (RDP) by calculating star number density in concentric rings. The RDP was then used to check whether a cluster candidate exhibits an obvious excess in the star number compared to the background. The RDP was used to determine the radius of the candidate cluster as well.

The core radius ($R_{\rm core}$) of each cluster candidate was acquired by fitting its RDP to the empirical King model (King 1962). Then $2 \times R_{\rm core}$ was adopted as the cluster visual radius R. Outside the visual radius, RDP slope becomes flat and stars within the visual radius are used for cluster parameter analysis. However, for faint and diffuse candidates ($R < 1.5'$), the fitted $R_{\rm core}$ is too small, so there are not enough stars within $R_{\rm core}$ that could be used in the CMD analysis and to derive cluster parameters. While for candidates with large $R_{\rm core}$, there would be many field stars contaminating the analysis. Finally, the stars used for the cluster parameter analysis are selected in the range of $1.5'' < R < 4.0''$.

For each candidate, we selected stars in a square region of 1.0 deg^2 around its calculated center. Photometric data from XSTPS-GAC, 2MASS and UCAC4 were used here. Based on its center coordinate and cluster radius determined above, we built optical CMDs of (r, $g-r$) and (i, $r-i$), and an infrared CMD of (J, $J-H$) for each cluster. The stars within the adopted radius R are used as member candidates and all stars outside $2R$ are used as the control field stars.

The estimations of age, distance and reddening for a cluster were done by fitting its CMD to a solar-

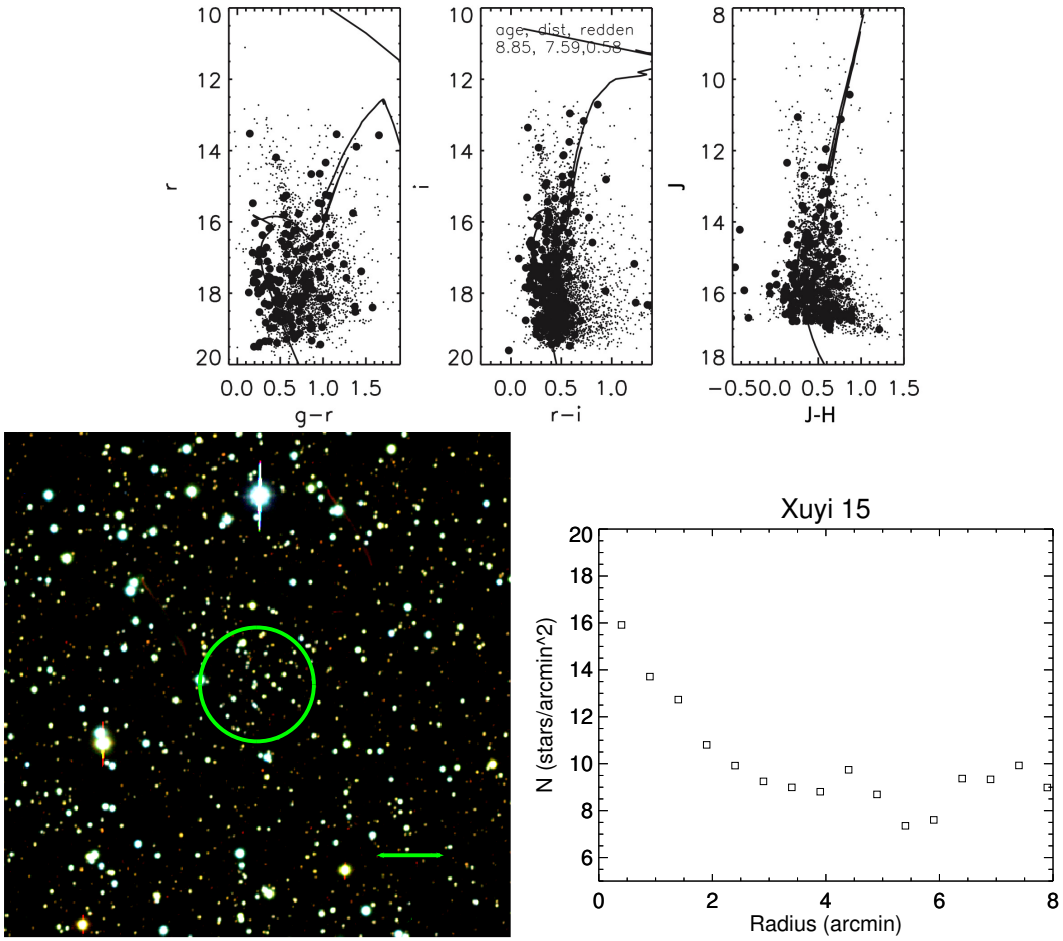

Fig. 5 Same as Fig. 2 but for cluster Xuyi 15. This is another example of an obvious cluster that shows a clear blue main sequence.

metallicity isochrone from Girardi et al. (2002). Mostly, isochrone fitting was done on the optical CMDs of $(r, g-r)$ and $(i, r-i)$. Comparisons were also made with the 2MASS $(J, J-H)$ CMD, especially for clusters whose bright stars, such as red giant branch stars, are saturated on XSTPS-GAC. In addition, only for large clusters, we adopted proper motions from UCAC4 to choose relatively robust cluster members before isochrone fitting. The final parameters were determined from the best fitting on the $(i, r-i)$ CMD. The parameter uncertainties were adopted from derived parameter differences between CMDs of $(i, r-i)$ and $(r, g-r)$.

Most known open clusters toward the GAC are relatively old, and each candidate discovered here is thought to be old enough to show its turn-off phase stars on the CMD. Therefore, by comparing with the background distribution, we identified the cluster-like feature, then manually picked the approximate CMD coordinate of turn-off stars as the initial offsets for each isochrone fitting. The adjustment of the theoretical isochrones on the CMD along the vertical axis represents the change of cluster visual distance, meaning the cluster reddens along the horizontal axis.

Even though there are several automatic isochrone fitting methods as mentioned in the Introduction, the isochrone fitting in this work was done manually. One reason is that almost all of these methods are suitable for well observed clusters, e.g. those having accurate and deep photometric measurements with plenty of cluster members, or with well measured proper motion. However, for diffuse or faint clusters, these approaches will produce large errors. Furthermore, each of these automatic methods will return a series of suitable parameter sets, which also needs one to determine the best set.

The isochrone fitting was carried out in the following steps. First, isochrones of $\log(age) = 7.00, 7.50, 8.00, 8.50, 9.00$ and 9.50 were selected as a basic isochrone set. Then through the rough fitting to basic isochrones

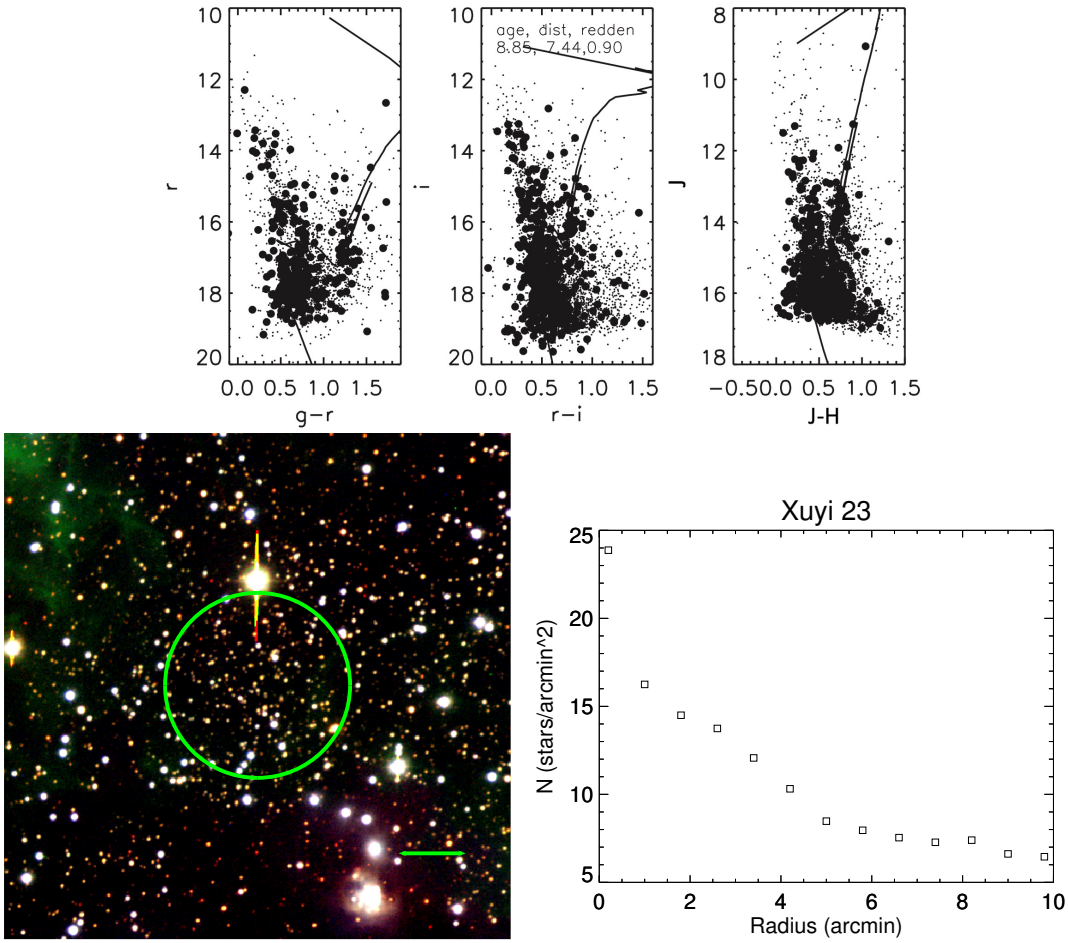

Fig. 6 Same as Fig. 2 but for cluster Xuyi 23. Xuyi 23 is an obscured cluster.

Table 1 Extinction Coefficients Used in the Unit of $E(B-V)$

Filter	Value	Color	Value
r	2.31	$g-r$	0.99
i	1.71	$r-i$	0.60
j	0.72	$j-h$	0.26

on the CMD, we chose the best one as the cluster's reference isochrone, and referred to this corresponding age as $age_{\rm ref}$. Second, based on the reference, isochrones between $age_{\rm ref}-0.3$ and $age_{\rm ref}+0.3$ in steps of 0.05 were adopted. In order to perform a more accurate isochrone fitting, the isochrones were shifted along the color and magnitude axes in steps of 0.02 and 0.1 mag, respectively. Typically, after tens of fitting steps, the parameters of a cluster can be properly determined. Then we repeated the same steps on other CMDs independently for comparison, so that we could find the best isochrone fitting and corresponding cluster parameters.

The reddening law from Yadav et al. (2011) was used to derive $E(B-V)$ and A_V for each cluster, and the extinction coefficients from Yuan et al. (2013), shown in Table 1, were adopted. Yuan et al. (2013) carefully performed reddening measurement based on photometric data from GALEX, SDSS, 2MASS and WISE, ranging from the far ultraviolet to the mid–infrared. More details can be found in that paper.

4 RESULTS AND DISCUSSION

In this work, great effort has been spent to inspect the 30 overdensity peaks, as well as 12 known clusters, and to derive their physical parameters. However, the physical parameters of six new cluster candidates and one known cluster cannot be derived properly, owing to the significant error in isochrone fitting. Apart from these, the remaining 24 new stellar overdensities turned out to be new cluster candidates and their parameters are listed in Table 2. The remaining 11 known clusters could be studied well and their parameters are listed in Table 3. All the well studied clusters are exhibited in Figures 2 –

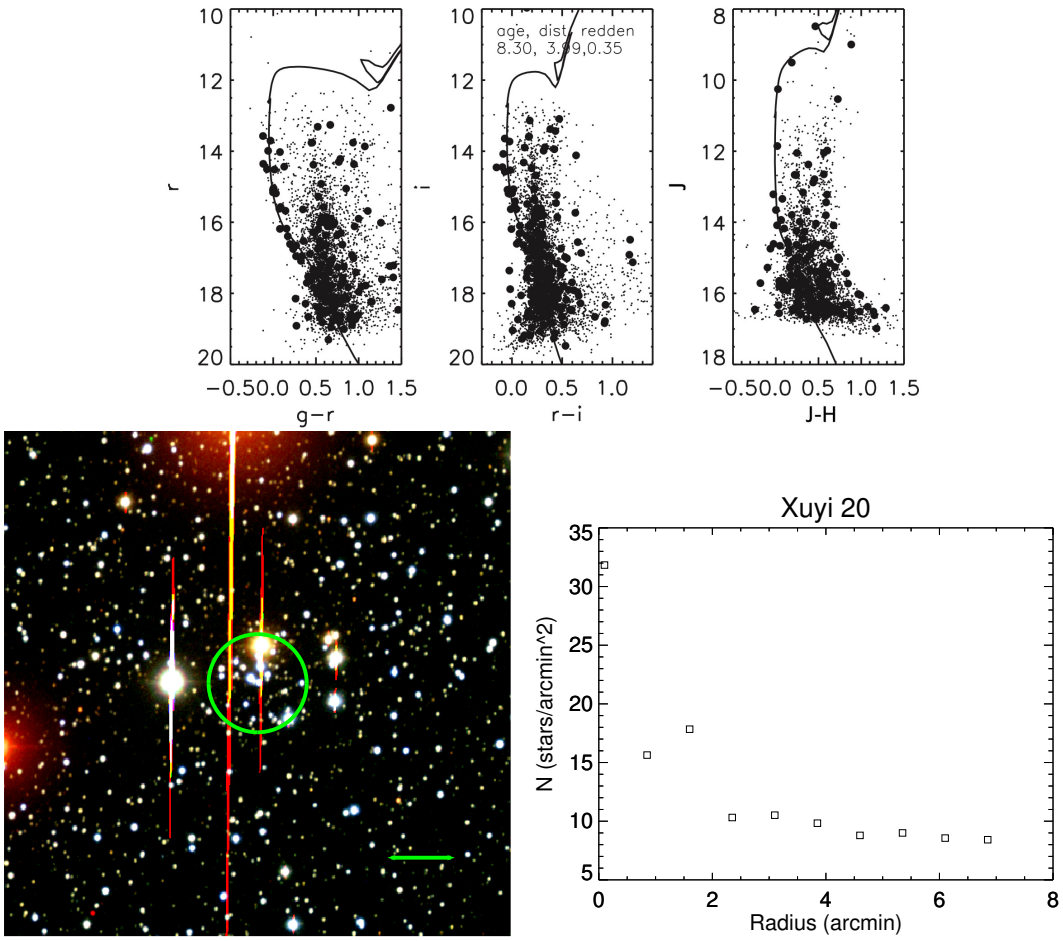

Fig. 7 Same as Fig. 2 but for cluster Xuyi 20. Xuyi 20 is a bright cluster.

10 with their CCD images, RDPs and $(r, g-r)$, $(i, r-i)$ and $(J, J-H)$ CMDs. For each CMD, the stars within the adopted radius R are considered as member candidates and displayed as filled black circles, while the stars outside $2\times$ R are considered as the control field stars and displayed as black dots.

Obvious Clusters. Teutsch 4, Alessi 50 and Juchert 23 are three obvious clusters in this study, showing clear spatial concentration, which can be separated well from the background stars. On their CMD, cluster member candidates display clear main sequence and giant branch trends. Parameters of these three clusters are investigated here for the first time. In Figure 2 we illustrate one of the obvious clusters, Alessi 50, with a clear main sequence and giant branch stars. The labeled parameters derived from the $(i, r-i)$ CMD are in good agreement with the parameters derived from the other two CMDs. The parameters and their uncertainties can be found in Table 3. Juchert 23 is relatively diffuse compared to the other two open clusters, but still can be discerned from the background. Alessi 50 is the closest among the three, suffering less dust reddening, while Teutsch 4 and Juchert 23 are located beyond 3.0 kpc.

The second kind of obvious cluster is a relatively compact cluster. These open clusters are dense and can be clearly seen on the CCD images. However, their main sequence stars are heavily mixed with field stars and their bright giant member stars are saturated on the CCD. Examples are Xuyi 24 as shown in Figure 3, and other clusters like these are Teutsch 60, Teutsch 20, Teutsch 59b and Xuyi 01. One should pay careful attention to these problems when identifying cluster features based on their optical CMDs. Fortunately, there are some clear giant stars on their infrared CMDs, which could help to constrain the accuracy of parameters. The parameters derived on the $(J, J-H)$ CMD are used as a reference to determine their labeled parameters on the $(i, r-i)$ CMD. The determined parameters show that all the five clusters

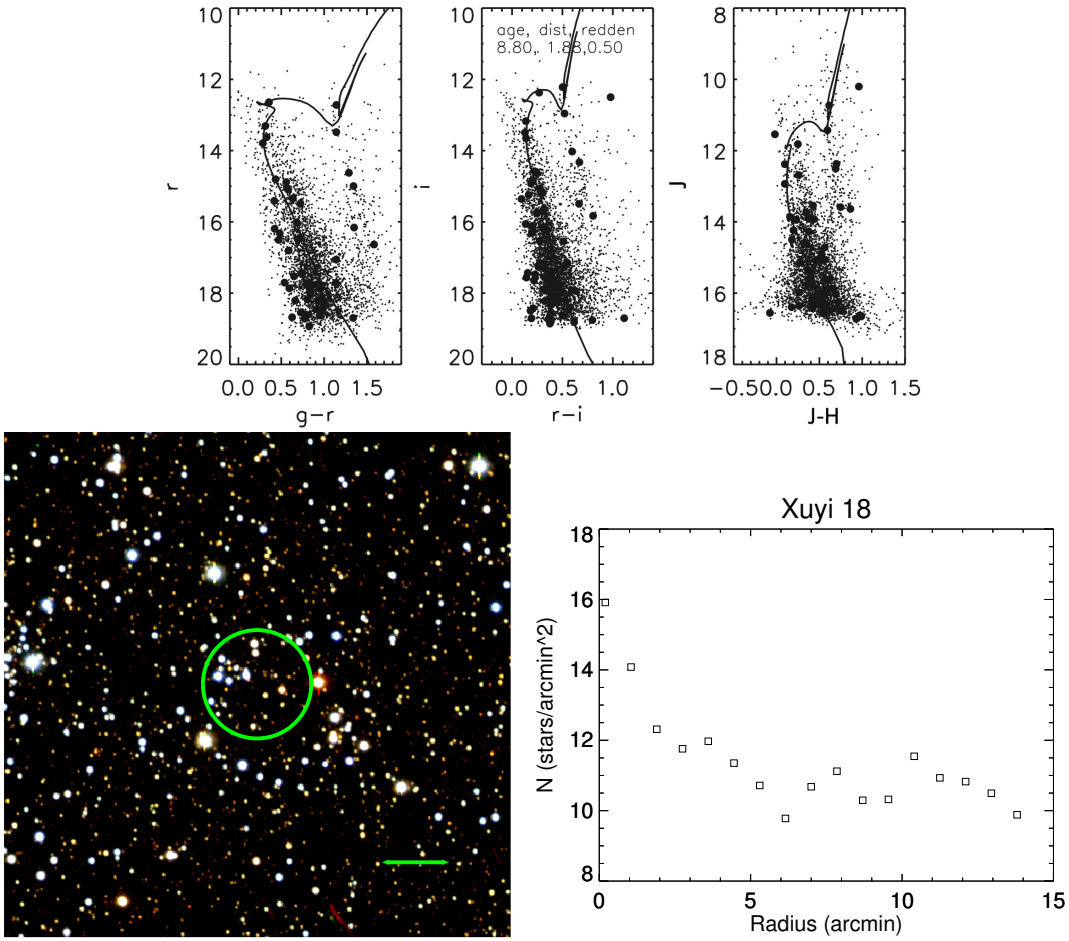

Fig. 8 Same as Fig. 2 but for cluster Xuyi 18.

are old open clusters, around 1 Gyr, and their distances range from 1.5 kpc to 3.2 kpc.

Obscured Clusters. Three faint clusters, Teutsch 58, Xuyi 21 and Xuyi 23, were discovered in this work. However, they are still dense enough to be evident on their images. Teutsch 58 is very red on its CCD image. Xuyi 21 is likely to be hidden by foreground stars. Xuyi 23 is very close to known cluster VdBergh 92, which is a large and bright cluster, as shown in the left panel of Figure 6. Red giant stars are detected in all three clusters, but their main sequence stars are contaminated by faint background stars. After analyses were carried out carefully, their ages were derived to be about 1 Gyr.

Bright Clusters. Three bright clusters, Xuyi 10, Xuyi 11 and Xuyi 20, are studied here. They were thought to be clusters of spikes at first, because their members are too bright. Fortunately they were picked out by visual inspection later. One bright cluster, Xuyi 20, is displayed in Figure 7. Their members are saturated on the XSTPS-GAC image, so 2MASS data were used to help derive their parameters. In addition, their ages are relatively young. Xuyi 11 turns out to be a very young cluster, with an age of about 100 Myr. Like clusters in the blue main sequence group, the main sequence of Xuyi 20 exhibits a very blue feature. Proper motions from UCAC4 were used to identify member stars and sharpen the cluster features on CMDs.

Inconspicuous Clusters. The clusters Xuyi 02–08, 12 and 14 are inconspicuous clusters, identified by some weak cluster-like features, but heavily contaminated by background stars. Two of them are shown in Figure 9 and Figure 10. The clusters Xuyi 03, Xuyi 05, Xuyi 06, Xuyi 07, Xuyi 08 and Xuyi 14 are identified by some clear giant branch stars. The clusters Xuyi 02, Xuyi 04, Xuyi 12 and Xuyi 14 are diffuse clusters. The cluster Xuyi 14 is identified by some turn-off phase stars, while clusters Xuyi 22–24 are identified by their narrow main sequence. Parameters for these clusters are carefully derived, and

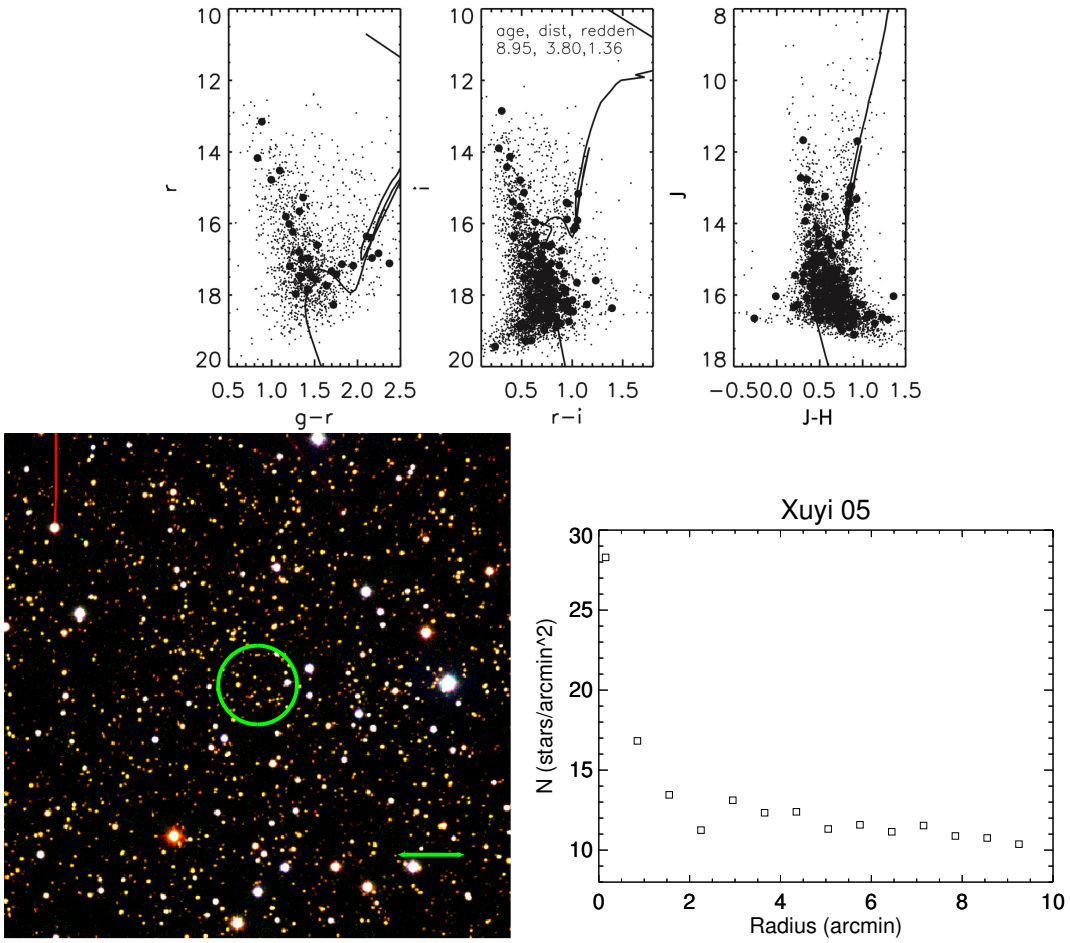

Fig. 9 Same as Fig. 2 but for cluster Xuyi 05. This is an example of an inconspicuous cluster, as described in the text, that has a heavily contaminated main sequence. Clusters like Xuyi 05 are recognized by some giant stars.

two times the parameter differences between $(i, r-i)$ and $(r, g-r)$ CMD are adopted as their uncertainties.

5 SUMMARY

Based on XSTPS-GAC photometry data, we searched for new star clusters on the stellar density maps. We added a weight factor to the density peak selection method, which was proven to be effective in removing false cluster candidates caused by star density fluctuations. Twenty-four new open cluster candidates were discovered in the region of the GAC. We manually derived parameters for these new clusters, and also derived parameters for another 11 previously known clusters found by Kronberger et al. (2006), who only provided cluster coordinates. The spatial distribution of these clusters in Galactic space is displayed in Figure 11, indicating these cluster candidates are located in the Galactic disk.

The obtained cluster parameters may be affected by our subjectivity, which may introduce some uncertainties, especially for clusters without a clear red giant branch or main sequence, like clusters Xuyi 09, Teutsch 58 and Xuyi 19. We carefully inspected each cluster on their CMD to ensure their member stars could be fitted well, and also checked them by using 2MASS data. Three obscured clusters were discovered and studied, indicating that deep infrared sky surveys like VVV are needed to find more clusters in the distant Galactic outer disk. Three bright clusters, Xuyi 10, Xuyi 11 and Xuyi 20, were located as well, suggesting nearby clusters still could be identified by careful searches. Furthermore, more small clusters will be found if we decrease the Gaussian width of the Koposov kernel used to find star density peaks, but it will be difficult to derive cluster parameters for these clusters, since their detected member stars will be just a few. On the other hand, almost all the

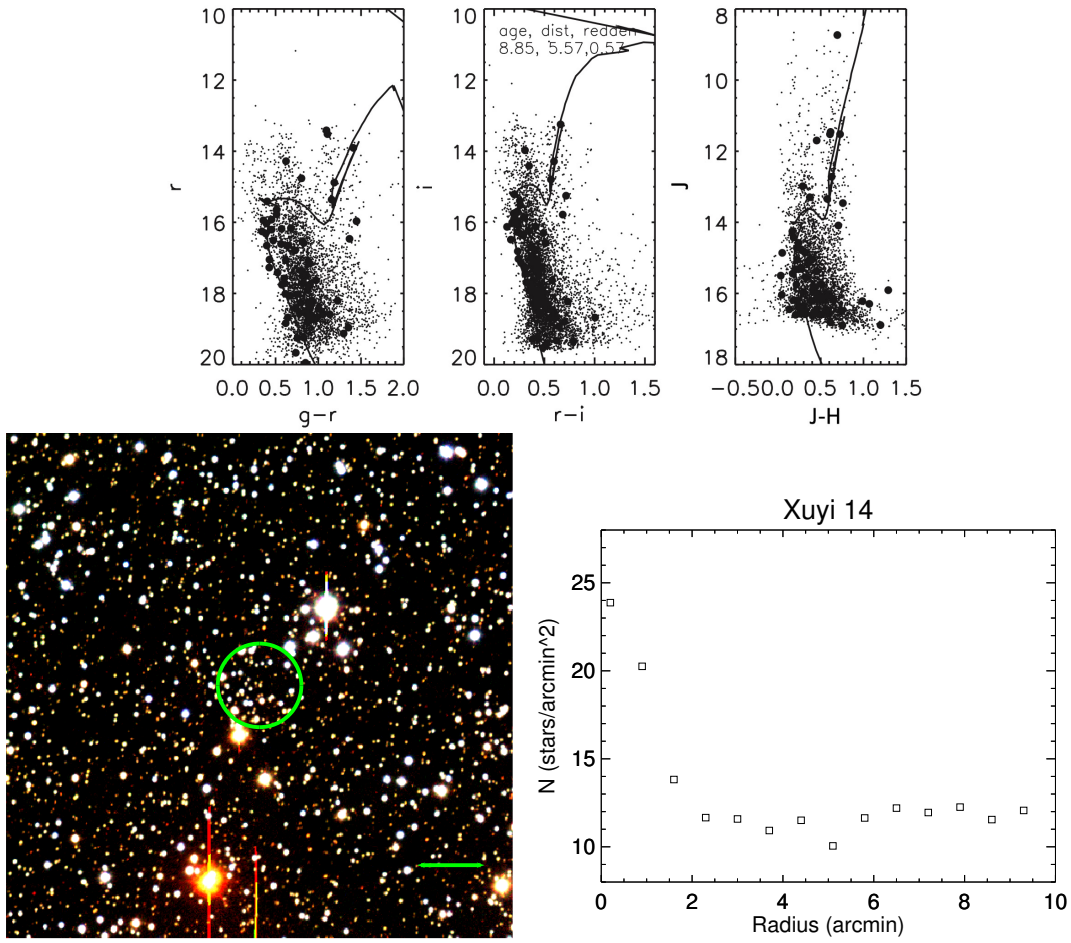

Fig. 10 Same as Fig. 2 but for cluster Xuyi 14. This is another example of an inconspicuous cluster, as described in the text, that shows a heavily contaminated main sequence. A cluster like Xuyi 14 is recognized by some stars on the turn-off phase.

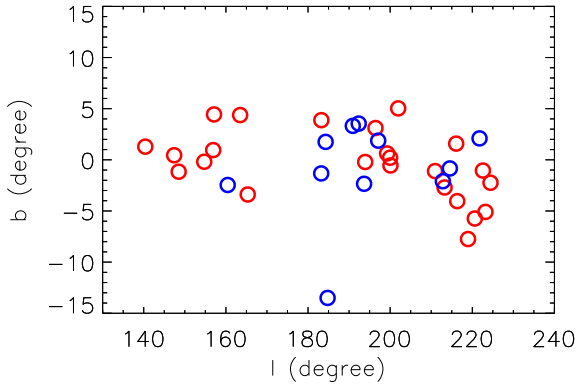

Fig. 11 The spatial distribution of all analyzed open cluster candidates in Galactic space. *Red circles* represent new open cluster candidates discovered in this work, while *blue circles* are the 11 previously known open clusters.

studied clusters in this work could be spectroscopically observed by LAMOST. Then, all newly discovered clusters and known clusters studied in this work will be important probes to investigate Galactic dynamics and evolution.

Table 2 Parameters of New Clusters

DSH ID	Name	RA J2000 (hh mm ss)	Dec J2000 (dd mm ss)	$R_{\rm core}$ (arcmin)	log Age (log yr)	$E(B-V)$ (mag)	Distance (kpc)
DSH J0314.8+5912	Xuyi 01	03 14 49	+59 12 56	1.98	8.85±0.05	0.82±0.44	2.09±0.30
DSH J0352.1+5230	Xuyi 02	03 52 04	+52 30 07	1.52	8.75±0.30	0.98±0.40	1.72±0.30
DSH J0353.2+5426	Xuyi 03	03 53 11	+54 26 38	0.84	8.70±0.40	1.09±0.02	2.64±0.60
DSH J0425.3+4901	Xuyi 04	04 25 17	+49 01 04	0.99	8.75±0.30	1.41±0.30	2.93±0.26
DSH J0439.3+4811	Xuyi 05	04 39 20	+48 11 57	1.17	8.95±0.30	1.36±0.18	3.80±0.95
DSH J0451.4+3859	Xuyi 06	04 51 23	+38 59 29	0.76	9.45±0.30	0.90±0.38	2.12±0.10
DSH J0456.5+5017	Xuyi 07	04 56 27	+50 17 41	0.71	9.00±0.20	0.91±0.22	4.44±0.68
DSH J0518.7+4510	Xuyi 08	05 18 41	+45 10 04	1.84	9.20±0.30	0.52±0.24	3.44±0.11
DSH J0608.3+2804	Xuyi 09	06 08 18	+28 04 13	3.09	8.55±0.15	0.37±0.08	5.78±1.92
DSH J0614.9+1645	Xuyi 10	06 14 57	+16 45 06	7.78	8.40±0.10	0.93±0.05	3.46±0.79
DSH J0625.7+1109	Xuyi 11	06 25 41	+11 09 56	8.93	7.85±0.15	0.39±0.02	1.46±0.11
DSH J0628.3+1135	Xuyi 12	06 28 16	+11 35 13	1.42	8.80±0.20	0.78±0.26	4.53±0.28
DSH J0628.4+1225	Xuyi 13	06 28 23	+12 25 54	1.62	8.70±0.10	0.62±0.19	3.31±0.57
DSH J0632.1+1605	Xuyi 14	06 32 04	+16 05 23	1.24	8.85±0.20	0.57±0.30	5.57±0.52
DSH J0634.6–0851	Xuyi 15	06 34 37	–08 51 59	1.69	8.85±0.15	0.58±0.37	7.59±0.57
DSH J0642.4–0130	Xuyi 16	06 42 23	–01 30 47	0.95	8.75±0.10	0.45±0.12	5.46±0.22
DSH J0643.2–0451	Xuyi 17	06 43 13	–04 51 46	1.73	8.55±0.05	0.48±0.12	9.16±1.23
DSH J0643.9+0116	Xuyi 18	06 43 52	+01 16 55	1.61	8.80±0.05	0.50±0.02	1.88±0.13
DSH J0644.9–0926	Xuyi 19	06 44 51	–09 26 02	0.98	8.75±0.15	0.56±0.03	5.99±1.09
DSH J0649.5+1202	Xuyi 20	06 49 28	+12 02 46	1.46	8.30±0.15	0.35±0.06	3.99±0.86
DSH J0651.9–1127	Xuyi 21	06 51 55	–11 27 42	0.66	8.90±0.20	1.37±0.42	5.58±0.06
DSH J0702.8–0204	Xuyi 22	07 02 49	–02 04 25	2.68	8.55±0.15	0.26±0.03	2.86±0.16
DSH J0704.6–1115	Xuyi 23	07 04 33	–11 15 33	2.75	8.85±0.15	0.90±0.14	7.44±0.94
DSH J0705.4–0903	Xuyi 24	07 05 24	–09 03 56	1.69	8.70±0.15	0.52±0.12	2.26±0.47

Table 3 Parameters of 11 Previously Known Clusters

DSH ID	Name	RA J2000 (hh mm ss)	Dec J2000 (dd mm ss)	$R_{\rm core}$ (arcmin)	log Age (log yr)	$E(B-V)$ (mag)	Distance (kpc)
DSH J0438.3+4317	Teutsch 4	04 38 16	+43 17 30	1.26	8.90±0.10	0.72±0.01	3.88±0.80
DSH J0507.7+1734	Juchert 23	05 07 40	+17 34 34	3.69	8.45±0.05	0.74±0.07	3.46±0.28
DSH J0548.0+2530	Teutsch 57	05 48 00	+25 30 03	0.89	8.60±0.10	0.72±0.15	6.59±0.17
DSH J0602.2+2607	Teutsch 92	06 02 15	+26 07 29	1.17	8.10±0.10	0.50±0.04	3.27±0.60
DSH J0606.6+1557	Teutsch 58	06 06 38	+15 57 19	0.83	9.00±0.15	1.59±0.36	4.11±1.27
DSH J0622.1+2104	Alessi 50	06 22 05	+21 04 31	1.07	9.10±0.25	0.57±0.25	2.55±0.20
DSH J0625.8+1954	Alessi 58	06 25 47	+19 54 19	1.55	8.20±0.10	0.50±0.02	3.82±0.48
DSH J0628.8+1456	Teutsch 20	06 28 48	+14 56 00	1.20	8.80±0.10	0.58±0.19	2.54±0.05
DSH J0643.8–0052	Teutsch 59b	06 43 49	–00 52 19	3.23	8.75±0.15	0.60±0.16	3.21±0.23
DSH J0651.4–0148	Teutsch 60	06 51 22	–01 49 00	1.37	9.15±0.15	0.36±0.02	1.55±0.38
DSH J0715.1–0653	Patchick 79	07 15 09	–06 53 23	2.50	8.50±0.10	0.31±0.04	4.59±0.22

Acknowledgements This work is supported by the National Natural Science Foundation of China (NSFC, Grant Nos. 11473001, 11233004, 11078006, 11633009 and 11273067), and by the Minor Planet Foundation of Purple Mountain Observatory. This work is also supported by the National Key Basic Research Program of China (2014CB845700) and by the China Postdoctoral Science Foundation (Grant No. 2017M610695).

The LAMOST Fellowship is supported by Special Funding for Advanced Users, budgeted and administrated by the Center for Astronomical Mega-Science, Chinese Academy of Sciences.

References

An, D., Johnson, J. A., Pinsonneault, M. H., et al. 2009, in Bulletin of the American Astronomical Society, 41, American Astronomical Society Meeting Abstracts #213, 204

Bertin, E., & Arnouts, S. 1996, A&AS, 117, 393

Bica, E., Bonatto, C., & Blumberg, R. 2006, A&A, 460, 83

Bonatto, C., & Bica, E. 2006, A&A, 455, 931
Borissova, J., Bonatto, C., Kurtev, R., et al. 2011, A&A, 532, A131
de Wit, W. J., Testi, L., Palla, F., & Zinnecker, H. 2005, A&A, 437, 247
Dias, W. S., Alessi, B. S., Moitinho, A., & Lépine, J. R. D. 2002, A&A, 389, 871
Froebrich, D., Scholz, A., & Raftery, C. L. 2007, MNRAS, 374, 399
Gilmore, G., & Reid, N. 1983, MNRAS, 202, 1025
Girardi, L., Bertelli, G., Bressan, A., et al. 2002, A&A, 391, 195
Kharchenko, N. V., Piskunov, A. E., Röser, S., Schilbach, E., & Scholz, R.-D. 2005, A&A, 438, 1163
Kharchenko, N. V., Piskunov, A. E., Schilbach, E., Röser, S., & Scholz, R.-D. 2012, A&A, 543, A156
Kharchenko, N. V., Piskunov, A. E., Schilbach, E., Röser, S., & Scholz, R.-D. 2013, A&A, 558, A53
King, I. 1962, AJ, 67, 274
Koposov, S. E., Glushkova, E. V., & Zolotukhin, I. Y. 2008, A&A, 486, 771
Kronberger, M., Teutsch, P., Alessi, B., et al. 2006, A&A, 447, 921
Lada, C. J., & Lada, E. A. 2003, ARA&A, 41, 57
Lasker, B. M., Lattanzi, M. G., McLean, B. J., et al. 2008, AJ, 136, 735
Liu, X.-W., Yuan, H.-B., Huo, Z.-Y., et al. 2014, in IAU Symposium, 298, Setting the Scene for Gaia and LAMOST, eds. S. Feltzing, G. Zhao, N. A. Walton, & P. Whitelock, 310
Majaess, D., Turner, D., Moni Bidin, C., et al. 2012, A&A, 537, L4
Minniti, D., Lucas, P. W., Emerson, J. P., et al. 2010, New Astron., 15, 433
Padmanabhan, N., Schlegel, D. J., Finkbeiner, D. P., et al. 2008, ApJ, 674, 1217
Portegies Zwart, S. F., McMillan, S. L. W., & Gieles, M. 2010, ARA&A, 48, 431
Roeser, S., Demleitner, M., & Schilbach, E. 2010, AJ, 139, 2440
Skrutskie, M. F., Cutri, R. M., Stiening, R., et al. 2006, AJ, 131, 1163
Stetson, P. B. 1987, PASP, 99, 191
Xiang, M. S., Liu, X. W., Yuan, H. B., et al. 2015, MNRAS, 448, 822
Yadav, R. K. S., Glushkhova, E. V., Sariya, D. P., et al. 2011, MNRAS, 414, 652
Yuan, H. B., Liu, X. W., & Xiang, M. S. 2013, MNRAS, 430, 2188
Zacharias, N., Finch, C. T., Girard, T. M., et al. 2013, AJ, 145, 44
Zhang, H.-H., Liu, X.-W., Yuan, H.-B., et al. 2013, RAA (Research in Astronomy and Astrophysics), 13, 490
Zhang, H.-H., Liu, X.-W., Yuan, H.-B., et al. 2014, RAA (Research in Astronomy and Astrophysics), 14, 456
Zhao, G., Zhao, Y.-H., Chu, Y.-Q., Jing, Y.-P., & Deng, L.-C. 2012, RAA (Research in Astronomy and Astrophysics), 12, 723